Iraqi Journal of Physics, 2024
https://doi.org/10.30723/ijp.v22i4.1287

Vol. 22, No. 4, PP.117-129
P-ISSN: 2070-4003
E-ISSN: 2664-5548

Optimization of Several Parameters Towards 30% Efficiency Perovskite Based Solar Cell Using SCAPS-1D Software

Burak Yahya Kadem[1a*] and Ehsan M. Abbas[2b]
[1]*College of Science, Al-Karkh University of Science, Baghdad, Iraq*
[2]*College of Health and Medical Technologies, Al-Shaab University, Baghdad, Iraq*
[a*]Corresponding author: drburakkadem@gmail.com

Abstract

A simulated perovskite solar cell based on a P3HT/MAPbI3/C60 structure is examined to achieve 30% PCE using SCAPS-1D software. Several aspects of A simulated perovskite solar cell based on a P3HT/MAPbI3/C60 structure are examined to achieve 30% PCE using SCAPS-1D software. Several aspects of the perovskite layer were evaluated, including the perovskite layer thickness, CB and VB effective density of state, band gap, and electron affinity. These factors greatly influence the device's performance. The best device based on the best-examined parameter has exhibited a PCE of 32.1% correlated with FF of 84.8%, V_{OC} of 1.23V and J_{SC} of 30.77 mA.cm^{-2}. Such a result is promising towards achieving high PCE for perovskite-based solar cells by optimizing several factors, including active layer thickness, energy band gap, electron affinity, and effective state density for CB and VB. However, the preparation conditions and other factors may render this result in the experimentally produced solar cells. A low effective DOS of ($1x10^{16}$m^{-3}) is desired for both CB and VB to achieve high solar cell performance.

Article Info.

Keywords:
SCAPS-1D, MAPbI3, Solar Cell, Perovskite, P3HT.

Article history:
Received: Apr. 30, 2024
Revised: Aug. 15, 2024
Accepted Aug. 17, 2024
Published:Dec.01,2024

1. Introduction

For decades, humans have depended on fossil fuels as the major sources of energy, despite their negative effects on the environment, mainly through the emission of greenhouse gases that contribute to climate change. To address this issue, it is imperative to prioritize the development of clean energy alternatives such as thermoelectric, wind, and photovoltaic energy on a large scale [1-3]. Among these alternatives, photovoltaic (PV) energy is particularly promising. It involves directly converting sunlight into electricity using PV cells. Solar cells typically consist of silicon-based N- and P-type semiconductors, which remain dominant due to their availability and stability, while their high production costs limit their accessibility to low-income communities. Perovskite solar cells (PSCs) offer a solution to this issue, meeting cost-effectiveness and efficiency criteria. Despite their potential, PSCs face challenges related to stability, both thermally and mechanically. Nevertheless, significant progress has been made in enhancing the efficiency of PSCs, increasing from 3% in 2006 to approximately 20% by 2020 [4]. Recently, a Power Conversion Efficiency (PCE) of 22.17% was reported for the SnO_2/$MAPbI_3$/NiO_X structure using SCAPS-1D Simulation [5]. Moreover, a simulated lead-free heterojunction double perovskite solar cell made of $CsGeI_2Br$/$CsGeI_3$ evaluated using SCAPS-1D software has achieved a PCE of 31.86% [6]. Nath et al. reported a PCE of 25% using lead-free halide double perovskites [7]. Practically, Cao et al. [8] reported a PCE of 19.42%. They have mentioned that defects influence the PCE and stability of perovskite solar cells. Therefore, to estimate a perovskite solar cell using SCAPS-1D software or any other simulation program, it is essential to consider the defects of the perovskite absorber layer [9].

The main aim of this study is to develop a high-performance perovskite solar cell with a simple structure and optimized parameters. Such a study could pave the way towards experimentally produced perovskite solar cells with efficiency exceeding 30%. This structure has not been investigated in detail, and for this reason, this study was carried out.

2. Device Model and Simulation Parameters

The simulation consists of (left contact/P3HT/$MAPbI_3$/C60/right contact) solar device under AM 1.5 G 1sun and 100 mW/cm^2 illumination, where Buckminsterfullerene (C60) was used as the Electron Transport Layer (ETL) [10], Poly(3-hexylthiophene) (P3HT) as the Hole Transport Layer (HTL) [11] and methyl ammonium lead iodide ($CH_3NH_3PbI_3$) as the absorber perovskite layer. SCAPS-1D software uses Poisson Eq. (1), continuity Eqs. (2) and (3) and carrier transport Eqs. (4) and (5) for electrons and holes to obtain the current density-voltage (J-V) characteristics:

$$\Delta\varepsilon\Delta\phi = = q(p - n + N_D^+ - N_A^-) \quad (\mathbf{1})$$

For electrons:

$$\Delta J_n = q(R - G) + q\frac{\partial n}{\partial t} \quad (\mathbf{2})$$

For holes:

$$\Delta J_p = q(R - G) + q\frac{\partial p}{\partial t} \quad (\mathbf{3})$$

For electrons:

$$J_n = D_n\frac{dn}{dx} + \mu_n n\frac{d\phi}{dx} \quad (\mathbf{4})$$

For holes:

$$J_p = D_p\frac{dp}{dx} + \mu_p p\frac{d\phi}{dx} \quad (\mathbf{5})$$

where ε is the dielectric constant, N_D and N_A are the donor and acceptor densities, respectively, p and n are the free holes and free electrons, ϕ is the electrostatic potential, J_n and J_p are the current densities for the electrons and the holes, respectively, R and G are the recombination and generation rates, respectively, and μ_n and μ_p are the electron and hole mobility, respectively. The simulated parameters of the materials used in this study are illustrated in Table 1.

Table 1: The parameters used in SCAPS-1D software to evaluate the device performance.

Parameters	P3HT [6]	MAPbI3 [5]	C60 [12]
Thickness (nm)	100	Variable (500-2000)	100
Band gap (eV)	1.7	Variable (1.4-1.8)	1.7
Electron affinity (eV)	3.5	Variable (3.8-4.2)	3.9
Dielectric permittivity	3	10	4.2
CB effective DOS ($1/cm^3$)	2.2×10^{18}	Variable (1×10^{16} -1×10^{19})	8×10^{19}
VB effective DOS ($1/ cm^3$)	2.2×10^{18}	Variable (1×10^{16} -1×10^{19})	1×10^{20}
Electron thermal velocity (cm/s)	1×10^{7}	1×10^{7}	1×10^{7}
Electron thermal velocity (cm/s)	1×10^{7}	1×10^{7}	1×10^{7}
Hole mobility ($cm^2/V.s$)	1.8×10^{-2}	1×10^{2}	8×10^{-2}
Electron mobility ($cm^2/V.s$)	1.8×10^{-3}	1×10^{2}	50
N_D ($1/cm^3$)	0	1×10^{9}	1×10^{17}
N_A ($1/cm^3$)	1×10^{18}	1×10^{9}	0
Defect energetic distribution	Single	Neutral	Single
Defect density (N_t) ($1/cm^3$)	1×10^{14}	1×10^{14}	1×10^{16}

The photovoltaic properties in the form of current density-voltage (J-V) dependence are usually used to calculate the fill factor (FF) and the power PCE according to the following equations [11]

$$\text{PCE}\ (\%) = \frac{J_{max}V_{max}}{P_{in}} \qquad (6)$$

$$\text{FF} = \frac{J_{max}V_{max}}{J_{sc}\ V_{oc}} \qquad (7)$$

where J_{sc} is the short-circuit current density ($mA.cm^{-2}$), V_{oc} is the open-circuit voltage (V), P_{in} is the incident light power and J_{max} ($mA.cm^{-2}$) and V_{max} (V) are the current density and voltage at the point of maximum power output in the J-V curves, respectively.

3. Results and Discussions

1.1. Effect of Active Layer Thickness

It is well-known that the active layer thickness is a crucial factor that effects the solar cell performance [13], for this reason different perovskite active layer thickness ranging from 500 to 2000 nm were studied to determine the best active layer thickness for the best solar cell performance. Simulated results, demonstrated in Fig.1(A-C), showed an enhancement in the devices' performance with increasing the active layer thickness.

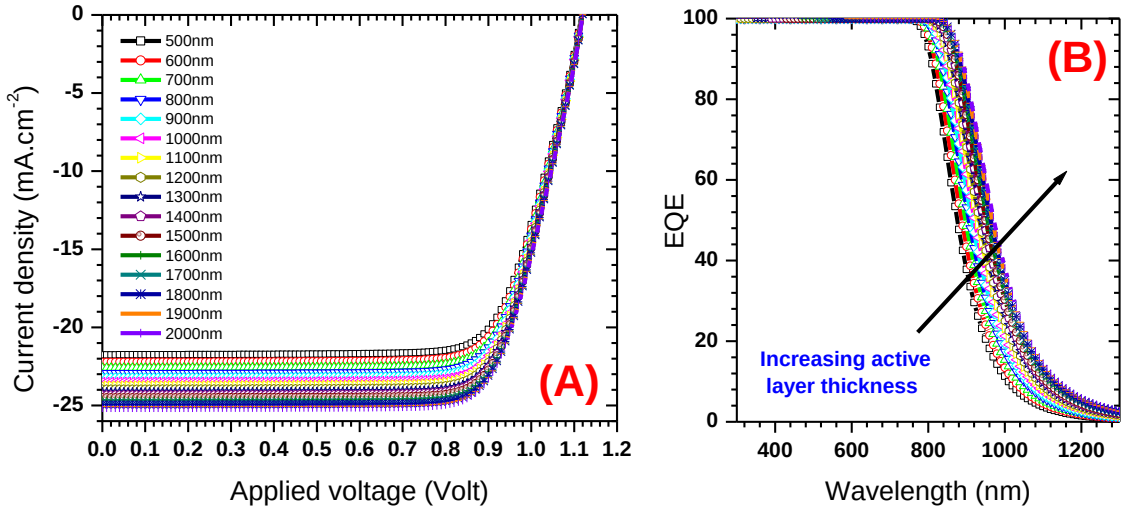

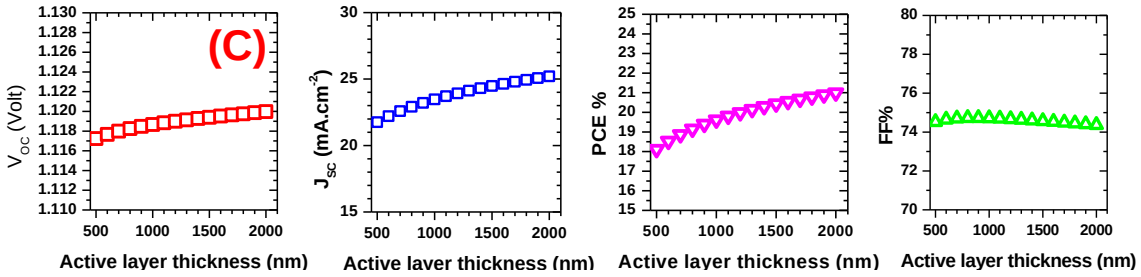

Figure 1: Solar cell characteristics based on different perovskite active layer thickness, (A) J-V curve, (B) EQE and (C) JV parameters V_{OC}, J_{SC}, FF and PCE as a function of different active layer thickness.

One aim of this study is to study the effect of the active layer thickness. As the active layer thickness increased, more photon was absorbed, and higher generation rate occurred. The increase in the current density is attributed to the increase in the absorption which is confirmed by the external quantum efficiency (EQE) spectra shown in Fig.1B. Such enhancement with increasing the active layer thickness contributes to high photo-generation, hence, high charge carriers [14]. Upon increasing the active layer thickness, the absorption edge is red-shifted towards higher wavelengths. Perovskite-based solar cells cover a broader range of wavelengths from 300 to 1300nm in the EQE spectra. The enhancement in EQE is confirmed by the J-V curve in Fig.1A, which improves J_{SC} by increasing the active layer thickness. Results shown in Fig.1C illustrate the variation in the solar cell parameters (V_{oc}, J_{sc}, FF, PCE) as a function of the active layer thickness. Results indicate that J_{SC} increases with increasing the active layer thickness to reach the maximum J_{SC} of 25.2 mA.cm^{-2} at an active layer thickness of 2000nm compared to 32.63 mA.cm^{-2} for the device with an active layer thickness of 500nm. S. Mehmood et al. [5] studied the effect of the absorber layer thickness of perovskite-based solar cells using SCAPS-1D software. They stated that the absorber thickness is essential to improve solar cell devices. PCE of 14.4% was reached with an active layer thickness of 450nm. Mandadapu et al. [15] stated the effect of varying the active layer thickness of $CH_3NH_3PbI_3$ perovskite from 100 to 600nm on PCE values. They found that the optimum active layer thickness was 300nm with PCE of 31.77%, J_{SC} of 25.60 mA.cm^{-2}, V_{OC} of 1.52V and FF of 81.58%. On the other hand, FF demonstrated no change when the active layer thickness was increased over 300nm. Mainly, FF is controlled by the shunt resistance (R_{sh}), which plays an important role in controlling the leakage current, and the series resistance (R_s), which is mainly, refers to the contact resistance between the active layer and the electrodes. Results shown in Fig.1A illustrate no change in both resistances upon increasing the active layer thickness. The effect of these resistances could interrupt the exciton dissociation, and therefore, higher charge carrier recombination occurs [16], which directly affects the fill factor [17]. It is worth noting that in this section, the series and shunt resistances are not considered in the simulation. FF has exhibited the values in the range of 74.3-74.7% for all samples. The V_{OC} is directly affected by serval parameters, including the energy and the Fermi level positions where V_{OC} is mainly determined by the difference between the HOMO $_{donor}$ and the LUMO $_{acceptor}$ [18].

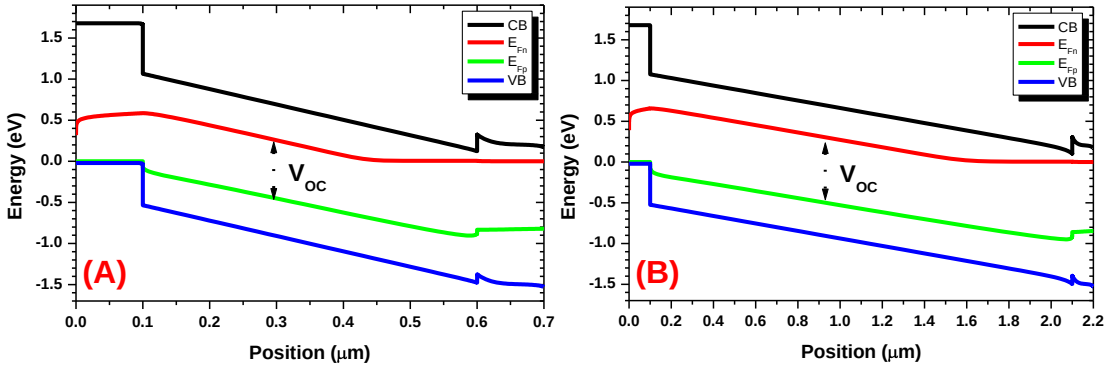

Figure 2: Energy level alignment for the used layers with active layer thicknesses (A) 500, and (B) 2000nm.

The energy level position with active layer thicknesses of 500nm (Fig.2A) were compared with those of 2000nm (Fig.2B) active layer thicknesses. The V_{oc} demonstrated a slight increase from 1.117V in the device with an active layer thickness of 500nm to 1.12V in the device with an active layer thickness of 2000nm. Such an increase is demonstrated in Fig.2, where the difference between the Fermi level position of electrons (E_{Fn}) and the Fermi level position of holes (E_{Fp}) is observed. This is attributed to enhancing the electric field strength across the thick layer [19]. PCE was used to evaluate the solar cell performance. Perovskite-based solar cells with an active layer thickness of 2000 nm showed a maximum PCE of 21% compared to 18.11% for solar cells with an active layer thickness of 500nm. PCE increased linearly with increasing the active layer thickness; this indicates higher photo-harvesting with higher thickness and, consequently, higher current density [20]. However, the charge carriers cannot reach the respective electrode due to inefficient charge carrier transport and increased recombination loss. As a result, the optimum active layer thickness is 2000nm with PCE of 21%, J_{SC} of 25.2 mA.cm^{-2}, FF of 74.4% and V_{OC} of 1.12V.

1.2. Different Band Gaps

The band gap (E_g) can be modified to achieve high absorption properties. Different methods are used to reach an optimum E_g with good absorption characteristics near the band edge without degradation of the charge collection [21]. The variation in perovskite E_g was attributed to altering the rotation of NH_3CH_3 (MA) molecules couples to the PbI_3 host, resulting in effective structural phase changes [22, 23]. Using the best active layer thickness of 2000nm, different E_g values for the perovskite layer were used starting from 1.4 to 1.8eV to evaluate the best E_g for the absorber perovskite layer. Results, demonstrated in Fig.3(A), show the J-V curves of the perovskite solar cells for different E_g values. The current density increased when E_g was decreased; such an increase is attributed to the increase in the absorption and the red shifting in the EQE spectra at the band edge when E_g was reduced to 1.4eV, as shown in Fig.3(B). The J_{SC} increased from 19.97 mA.cm^{-2} to J_{SC} of 30.77 mA.cm^{-2} when the E_g is decreased from 1.8 to 1.4eV. This enhancement in the current density is attributed to the enhancement in the absorption at the band edge of the EQE spectra with strong red shift (see Fig.3B). The absorption enhancement is ascribed to the rotation of MA molecule which enhances absorption characteristics with decreasing E_g [24].

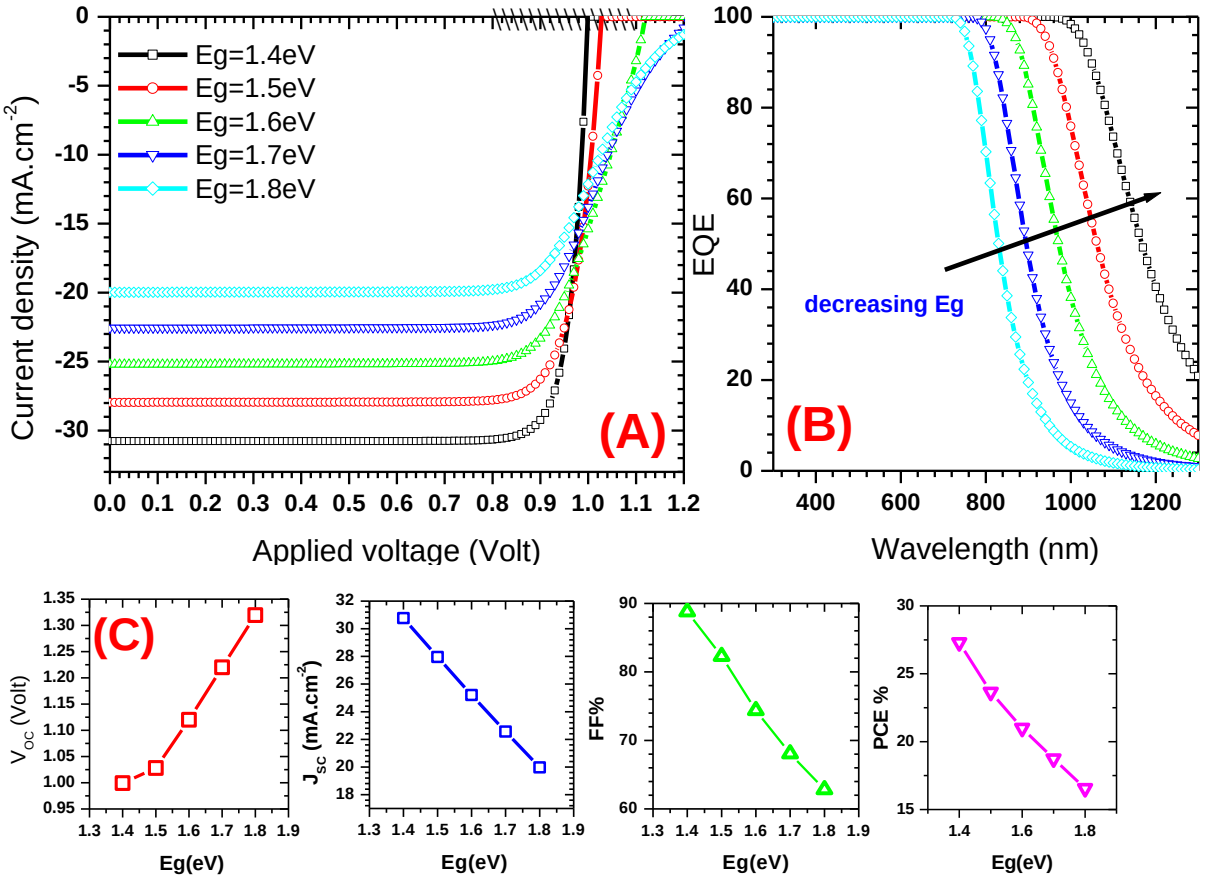

Figure 3: Solar cell characteristics based on different perovskite band gap, (A) J-V curve, (B) EQE, (C) JV parameters V_{OC}, J_{SC}, FF and PCE as a function of different active layer band gaps, and (D) Energy level alignments of the perovskite based solar cells with E_g=1.4eV and E_g=1.8eV.

The increase in the current density and the red shift of EQE with E_g of 1.4eV resulted in PCE as high as 27.3% compared to PCE of 16.56% for the device with E_g of 1.8eV. Such a result was associated with a higher FF of 88.8% when E_g was 1.4eV compared to FF of 62.8% when E_g was 1.8eV. The decrease in FF with increasing E_g is attributed to the increase in the recombination losses [25]. The high PCE when E_g was 1.4eV is mainly accredited to the increase in FF and J_{SC} [26]. Furthermore, the decrease in FF when E_g was increased to 1.8eV is also attributed to the R_S, which results in the deterioration of the overall solar cell performance. The perovskite solar cell with E_g equal or higher than 1.7eV results in higher R_S. It was reported that R_S largely affects the solar cell efficiency based on the semiconductor bandgap [27]. Usually, materials with large E_g have high resistivity and low conductivity, while materials with small E_g have low resistivity and high conductivity. A noticeable improvement in the photovoltaic performance of the perovskite-based solar cell can be observed when E_g of the absorber material is reduced. This enhancement mainly arises from improving PCE, FF and J_{SC}. On the other hand, increasing Eg directly affects serval parameters, including Fermi level position as well as conduction and valance bands position, as shown in Fig.3D. Therefore, V_{OC} is altered with changing E_g (ΔV_{OC}= Eg/qV_{OC}) [28]. V_{OC} is mainly assessed by the difference between the HOMO $_{donor}$ and the LUMO $_{acceptor}$ [18]. From Fig.3(C), the energy of the conduction band has shifted down to about 0.4eV when E_g increased from 1.4eV to 1.8eV. This shift is in agreement with increasing V_{OC}

from 0.99 V when E_g is 1.4eV to 1.32 V when E_g is 1.8eV. As a result, with the optimum active layer thickness of 2000nm and optimum E_g of 1.4eV, the device exhibited a PCE of 27.3%, J_{SC} of 30.77 mA.cm^{-2}, FF of 88.8% and V_{OC} of 0.99V.

1.3. Different Electron Affinity

To simulate the effects of perovskites' electron affinity (EA) on the solar cells performance, the best active layer thickness of 2000nm and the best E_g of the absorber layer of 1.4eV were used in this section. The EA is associated directly with LUMO, and it represents the energy required to raise a free electron from the bottom of the LUMO to the vacuum level. Fig.4(A and B) shows the energy level diagram of the perovskite solar cell with different EA level. A well-matched EA with electron and hole transport layers enhances hole/electron injection/blocking from the perovskite to the respective transport layers [29, 30]. The EA values used in this section ranged from 3.8eV to 4.2eV. The simulated energy level of P3HT/MAPbI3/C60 solar cell is demonstrated in Fig.4(C).

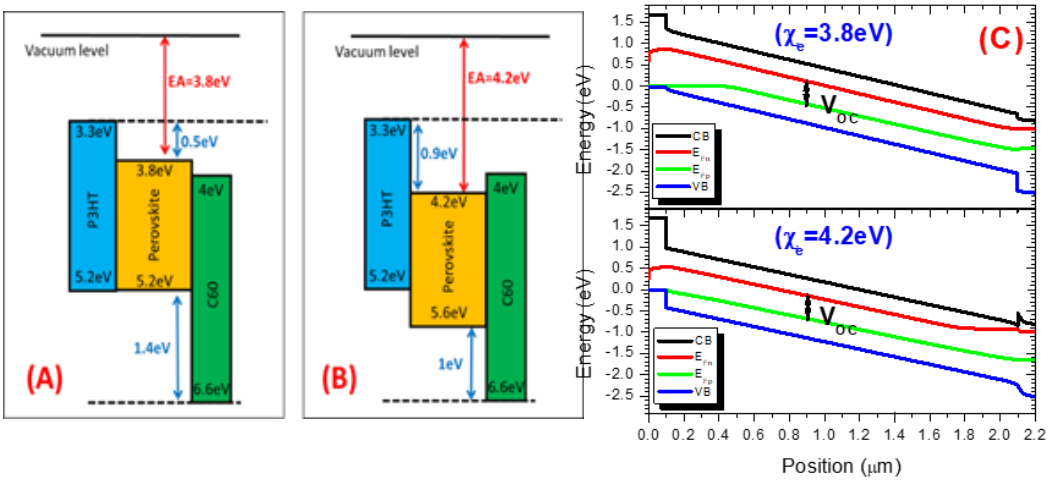

Figure 4: Energy band diagram of the perovskite solar cell (A) EA=3.8eV, (B) EA=4.2eV and (C) Energy bands bending simulated by SCAPS-1D software for both EA of 3.8eV and 4.2eV.

Fig.5(A) shows the J-V curves of the devices with different EA. It is obvious that the V_{OC} demonstrated a decrease when EA increased, whereas J_{SC} exhibited no change in its value; results are illustrated in Fig.5(B). The electron/hole injection barrier between the perovskite layer and the C60 layer was altered when EA decreased from 4.2eV to 3.8eV relative to the vacuum level. This resulted in different E_{Fp} and E_{Fn} through the device. This variation has altered HOMO and LUMO levels position and, therefore, higher V_{OC} resulted [31]. FF remains unchanged with changing EA values. However, it was reduced at a higher EA value of 4.2eV, and this has mainly been attributed to the interface properties and the exciton dissociation into free charge carriers [29]. The best solar cell device in this section was based on EA of 3.8eV with PCE of 26.95%, FF of 82.3%, J_{SC} of 30.77 mA.cm^{-2} and V_{OC} of 1.06V. When V_{oc} and FF decreased while J_{sc} remained constant, PCE decreased, and this indicates underlying issues with the cell's internal characteristics, even though its ability to generate current from light (as reflected by J_{sc}) remains unchanged. The cell is still absorbing light and generating charge carriers, but it is less effective at converting these carriers into electrical energy due to internal resistance.

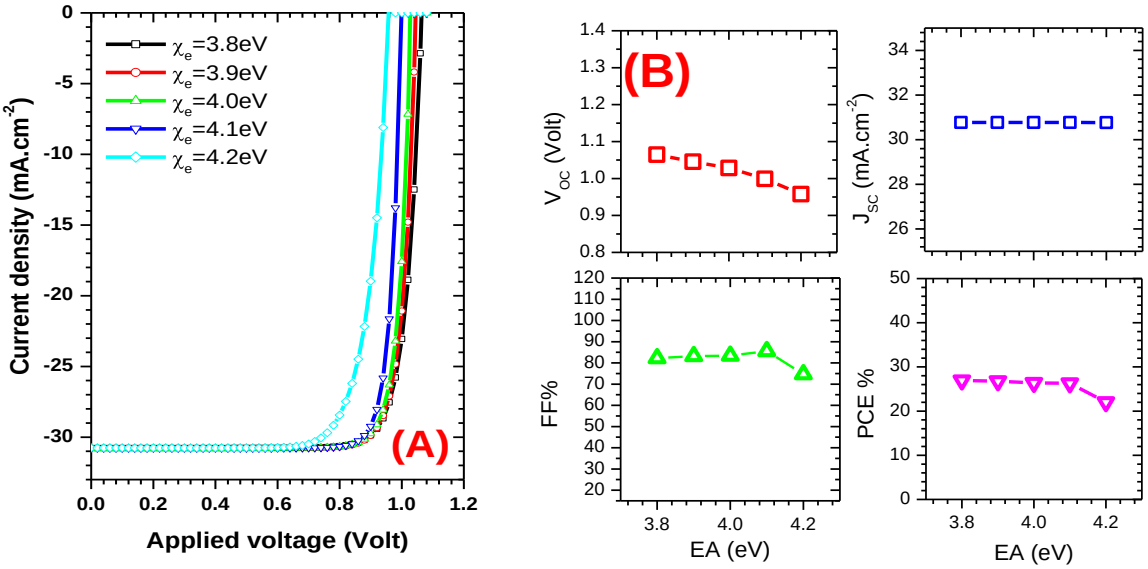

Figure 5: Solar cell characteristics based on different perovskite EA, (A) J-V curve, (B) JV parameters V_{OC}, J_{SC}, FF and PCE as a function of perovskite EA, and (C) Energy level alignments of the perovskite based solar cells with EA=3.8eV and EA=4.2eV.

1.4. Different CB and VB Effective Density of State

The effective density of states (DOS) for the conduction band (CB) and the valance band (VB) of the perovskite layer was varied from 1×10^{16} to 1×10^{19} cm^{-3}; its effect on the J-V curve is illustrated in Fig.6(A and B). The increase of DOS resulted in the reduction of the device performance, as shown in Fig.6(C); PCE decreased when the effective DOS of the CB and VB increased; this decrease is mainly attributed to the reduction in FF and V_{OC}. However, there was a slight change in the J_{SC} value with increasing DOS. As mentioned earlier, V_{OC} is mainly estimated by the difference between the HOMO $_{donor}$ and the LUMO $_{acceptor}$ [18].

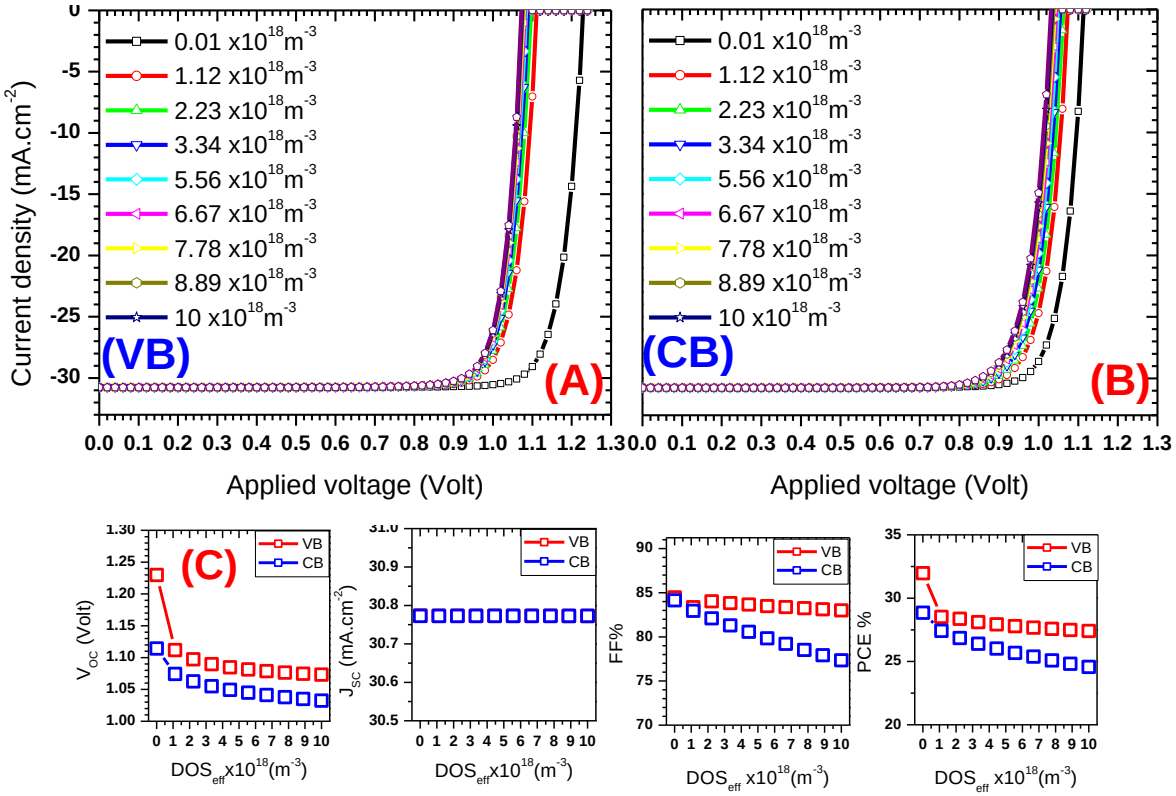

Figure 6: Solar cell characteristics (A) VB effective DOS (B) CB effective DOS and (C) JV parameters V_{OC}, J_{SC}, FF and PCE as a function of DOS.

Fig.7(A) shows the higher effective DOS of VB (1×10^{19} cm^{-3}), and Fig.7(B) shows the higher effective DOS of CB (1×10^{19} cm^{-3}). An illustration of the shift in the Fermi level in both cases is presented in Fig.7(C). This increase in the effective DOS of CB and VB resulted in shifting E_{Fn} and E_{Fp} deeper in the energy gap and, hence, lowering V_{oc}. Li et al. [32] have determined V_{oc} as a function of E_F using this equation $V_{oc}= (E_{Fn}-E_{FP})/q$. The best device performance with the lowest effective DOS of CB showed PCE of 28.85%, V_{oc} of 1.11V, J_{sc} of 30.77 $mA.cm^{-2}$ and FF of 84.14%. While the best device performance with the lowest effective DOS of VB showed PCE of 31.97%, V_{oc} of 1.13V, J_{sc} of 30.77 $mA.cm^{-2}$ and FF of 84.47%. Therefore, a low effective DOS is desired for both CB and VB to achieve high solar cell performance.

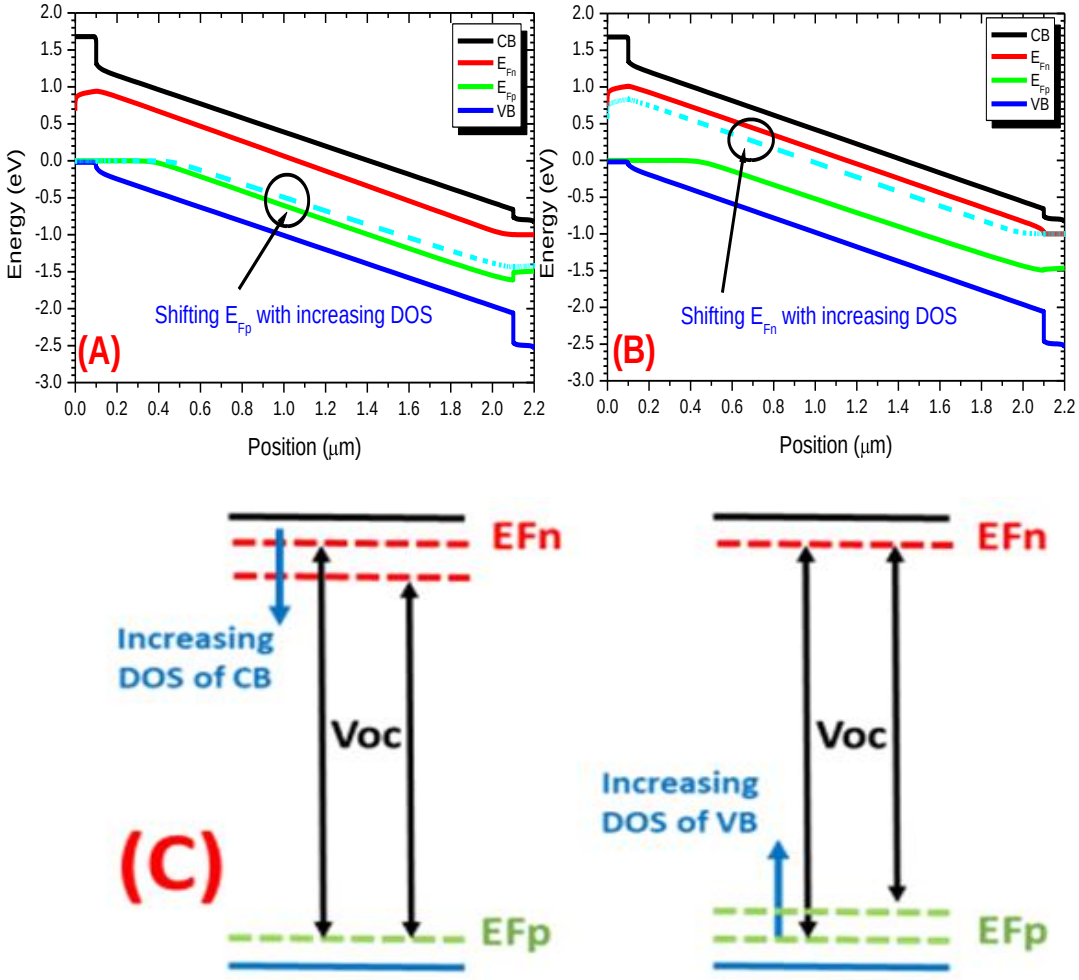

Figure 7: Energy band diagram of the perovskite solar cell (A) higher VB effective DOS and (B) higher CB effective DOS and (C) band diagram for both cases VB and CB effective DOS.

1.5. Different Temperature

In this section, the best active layer thickness of 2000nm, E_g of 1.4eV, EA of 3.8eV and DOS for CB and VB of 1×10^{19} cm^{-3} were used; the device performance was evaluated as a function of the working temperature in the range of 300K - 360K. J-V curve of the studied devices is illustrated in Fig.8(A) at different working temperatures. Increasing temperature decreased V_{OC} linearly, as shown in Fig.8(B) [33]. This decrease is attributed to the shifting of E_{Fn} and E_{Fp} deeper inside the energy gap, resulting in lower V_{oc}, as shown in Fig.8(C). Moreover, increasing temperature decreased PCE and FF, resulting in lower performance. Whereas J_{sc} remains almost stable. Similar results were obtained by Mamta et

al. for a Sb_2Se_3-based solar [34]. The best working temperature was 300K with PCE of 32.1%, V_{oc} of 1.23V, J_{sc} of 30.77 mA.cm^{-2} and FF of 84.8%.

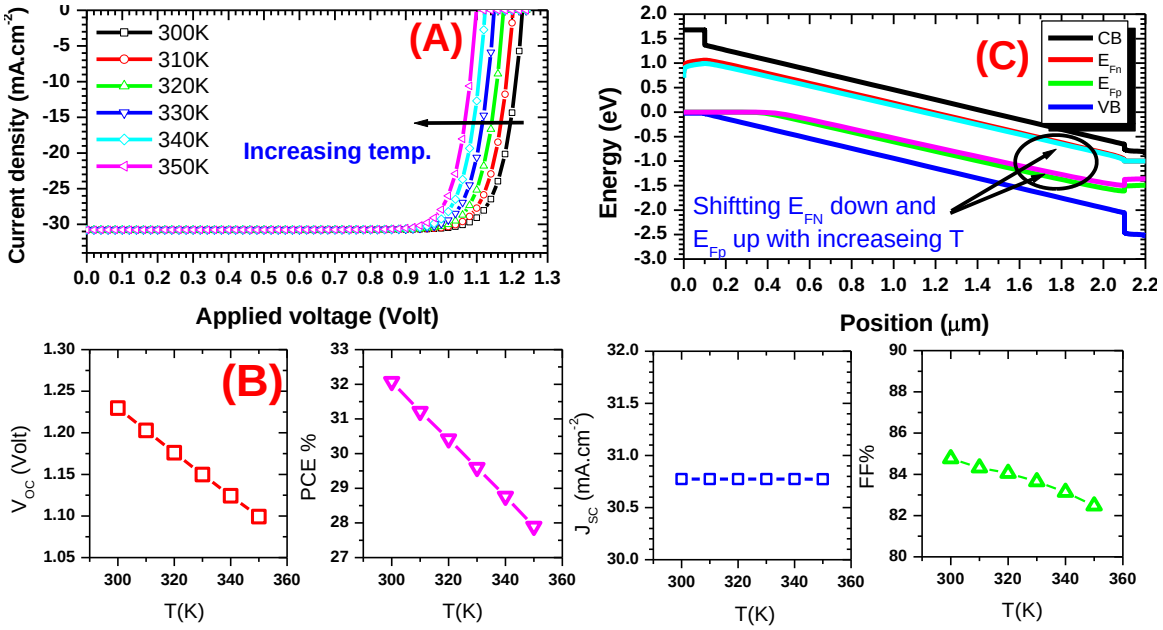

Figure 8: Solar cell characteristics (A) J-V curve, (B) JV parameters V_{OC}, J_{SC}, FF and PCE as a function of temperature and (C) Energy level position for the highest temperature used 350 ℃.

1.6. The Best Performance

The best device based on the best-evaluated parameters is introduced, and the J-V characteristics of this device are shown in Fig.9(A), EQE is shown in Fig.9(B) and energy band alignment is shown in Fig.9(C). The simulated parameters of this device are illustrated in Table 2. The best device exhibited a PCE as high as 32.1% correlated with FF of 84.8%, V_{oc} of 1.23V and J_{sc} of 30.77 mA.cm^{-2}. Such a result is promising for achieving high PCE for perovskite-based solar cells by optimizing several factors, including active layer thickness, energy band gap, electron affinity, and effective density of state for CB and VB. However, for the experimentally produced solar cells, the preparation conditions and other factors may render this result.

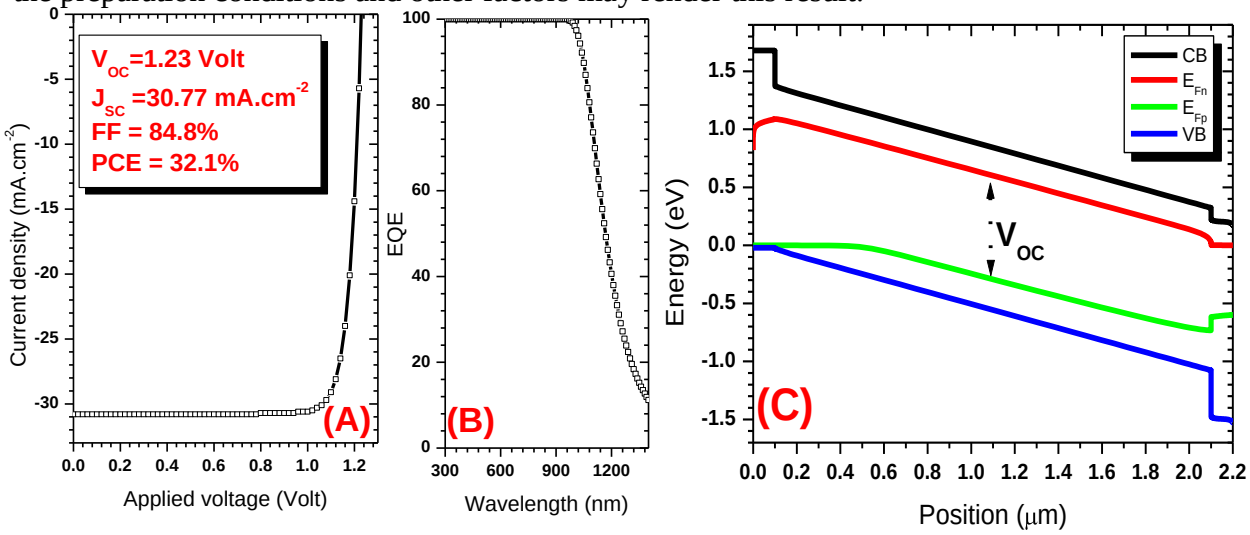

Figure 9: Solar cell characteristics of the best device based on best parameters investigated in this study (A) J-V curve, (B) EQE and (C) Energy level alignments.

Table 2: The best device parameters used in SCAPS-1D software to evaluate the device performance.

Parameters	P3HT	MAPbI3	C60
Thickness (nm)	100	2000	100
Band gap (eV)	1.7	1.4	1.7
Electron affinity (eV)	3.5	3.8	3.9
Dielectric permittivity	3	10	4.2
CB effective DOS (1/cm^3)	2.2× 10^{18}	1× 10^{16}	8× 10^{19}
VB effective DOS (1/ cm^3)	2.2× 10^{18}	1× 10^{16}	1× 10^{20}
Electron thermal velocity (cm/s)	1× 10^7	1× 10^7	1× 10^7
Electron thermal velocity (cm/s)	1× 10^7	1× 10^7	1× 10^7
Hole mobility (cm^2/Vs)	1.8× 10^{-2}	1× 10^2	8× 10^{-2}
Electron mobility (cm^2/Vs)	1.8× 10^{-3}	1× 10^2	50
N_D (1/cm^3)	0	1× 10^9	1× 10^{17}
N_A (1/cm^3)	1× 10^{18}	1× 10^9	0
Defect energetic distribution	Single	Neutral	Single
Defect density (N_t) (1/cm^3)	1× 10^{14}	1× 10^{14}	1× 10^{16}

4. Conclusions

In this study, the simulated perovskite-based solar cell of P3HT/MAPbI3/C60 structure was examined using SCAPS-1D software. Several parameters were examined for the perovskite layer to achieve high PCE, including the perovskite layer thickness, CB and VB effective density of state, band gap, and electron affinity. The optimum active layer thickness was 2000nm with PCE of 21%, J_{SC} of 25.2 mA.cm^{-2}, FF of 74.4% and V_{oc} of 1.12V. Further enhancement was achieved when the optimum perovskite band gap of 1.4eV was examined with PCE of 27.3%, J_{sc} of 30.77 mA.cm^{-2}, FF of 88.8% and V_{oc} of 0.99V. Electron affinity evaluation also had great effects on the device performance when the optimum electron affinity of 3.8eV was used with PCE of 26.95%, FF of 82.3%, J_{SC} of 30.77 mA.cm^{-2} and V_{oc} of 1.06V. The best device performance with the lowest effective dos of cb of 1x10^{16}m^{-3} showed pce of 28.85%, V_{oc} of 1.11V, J_{sc} of 30.77 mA.cm^{-2} and FF of 84.14%. While the best device performance with the lowest effective DOS of VB of 1x10^{16}m^{-3} showed PCE of 31.97%, V_{oc} of 1.13V, J_{sc} of 30.77 mA.cm^{-2} and FF of 84.47%. Therefore, a low effective DOS of (1x10^{16}m^{-3}) is desired for both CB and VB to achieve high solar cell performance. The best device based on the best-examined parameter has exhibited a PCE of 32.1% correlated with FF of 84.8%, V_{oc} of 1.23V and J_{sc} of 30.77 mA.cm^{-2}. This enhancement has been attributed to the variation in the Fermi level position, which influences the V_{oc} and the enhancement in the current density.

Conflict of interest

Authors declare that they have no conflict of interest.

References

1. A. D. Kapim, C. A. Nangmetio, and N. J. Kuatche, J. Elect. Mat. **52**, 951 (2023). DOI: 10.1007/s11664-022-10072-4.
2. A. Kumar, M. Z. U. Khan, B. Pandey, and S. Mekhilef, Gyan. J. Eng. Tech. **4**, 29 (2018). DOI: 10.21058/gjet.2018.42004
3. F. B. Pelap, E. K. Tagne, and A. D. K. Kenfack, J. Renew. Ener. **24**, 25 (2021). DOI: 10.54966/jreen.v24i1.971.
4. Y. Zhang, G. Grancini, Y. Feng, A. M. Asiri, and M. K. Nazeeruddin, ACS Ener. Lett. **2**, 802 (2017). DOI: 10.1021/acsenergylett.7b00112.
5. S. Mehmood, Y. Xia, F. Qu, and M. He, Energies **16**, 7438 (2023). DOI: 10.3390/en16217438.

6. A. D. K. Kenfack, N. M. Thantsha, and M. Msimanga, Solar **3**, 458 (2023). DOI: 10.3390/solar3030025.
7. B. Nath, B. Pradhan, and S. K. Panda, N. J. Chem. **44**, 18656 (2020). DOI: 10.1039/D0NJ03642K.
8. Y. Cao, Z. Liu, W. Li, Z. Zhao, Z. Xiao, B. Lei, W. Zi, N. Cheng, J. Liu, and Y. Tu, Sol. Ener. **220**, 251 (2021). DOI: 10.1016/j.solener.2021.03.055.
9. F. Wang, S. Bai, W. Tress, A. Hagfeldt, and F. Gao, NPJ Flex. Elect. **2**, 22 (2018). DOI: 10.1038/s41528-018-0035-z.
10. C. Xu, Y. Zhang, P. Luo, J. Sun, H. Wang, Y.-W. Lu, F. Ding, C. Zhang, and J. Hu, ACS Appl. Ener. Mat. **4**, 5543 (2021). DOI: 10.1021/acsaem.1c00226.
11. B. Y. Kadem, R. G. Kadhim, and H. Banimuslem, J. Mat. Sci. Mat. Elect. **29**, 9418 (2018). DOI: 10.1007/s10854-018-8974-7.
12. J. Arayro, R. Mezher, and H. Sabbah, Coatings **13**, 1258 (2023). DOI: 10.3390/coatings13071258.
13. L. Et-Taya, A. Benami, and T. Ouslimane, Sustainability **14**, 1916 (2022). DOI: 10.3390/su14031916.
14. L. Et-Taya, T. Ouslimane, and A. Benami, Sol. Ener. **201**, 827 (2020). DOI: 10.1016/j.solener.2020.03.070.
15. U. Mandadapu, S. V. Vedanayakam, and K. Thyagarajan, Indian J. Sci. Tech. **10**, 65 (2017). DOI: 10.17485/ijst/2017/v11i10/110721.
16. H. W. Lee, S. Biswas, Y. Lee, and H. Kim, IEEE Inter. Thin. J. **10**, 15923 (2023). DOI: 10.1109/JIOT.2023.3267098.
17. M. K. Al-Hashimi, B. Y. Kadem, and A. K. Hassan, J. Mat. Sci. Mat. Elect. **29**, 7152 (2018). DOI: 10.1007/s10854-018-8703-2.
18. B. Kadem, A. Hassan, and W. Cranton, J. Mat. Sci. Mat. Elect. **27**, 7038 (2016). DOI: 10.1007/s10854-016-4661-8.
19. N. Shrivastav, J. Madan, R. Pandey, and A. E. Shalan, RSC Advances **11**, 37366 (2021). DOI: 10.1039/D1RA06250F.
20. M. S. Islam, IEEE Access **9**, 130502 (2021). DOI: 10.1109/ACCESS.2021.3110508.
21. C. Wehrenfennig, G. E. Eperon, M. B. Johnston, H. J. Snaith, and L. M. Herz, Adv. Mater. **26**, 1584 (2014). DOI: 10.1002/adma.201305172.
22. K. P. Ong, T. W. Goh, Q. Xu, and A. Huan, J. Phys. Chem. A **119**, 11033 (2015). DOI: 10.1021/acs.jpca.5b09884.
23. C. Motta, F. El-Mellouhi, S. Kais, N. Tabet, F. Alharbi, and S. Sanvito, Nat. Commun. **6**, 7026 (2015). DOI: 10.1038/ncomms8026.
24. K. P. Ong, S. Wu, T. H. Nguyen, D. J. Singh, Z. Fan, M. B. Sullivan, and C. Dang, Sci. Rep. **9**, 2144 (2019). DOI: 10.1038/s41598-018-38023-2.
25. C. M. Wolff, P. Caprioglio, M. Stolterfoht, and D. Neher, Adv. Mater. **31**, 1902762 (2019). DOI: 10.1002/adma.201902762.
26. K. Wang, C. Liu, P. Du, J. Zheng, and X. Gong, Ener. Envir. Sci. **8**, 1245 (2015). DOI: 10.1039/C5EE00222B.
27. A. Vossier, F. Gualdi, A. Dollet, R. Ares, and V. Aimez, J. Appl. Phys. **117**, 015102 (2015). DOI: 10.1063/1.4905277.
28. M. Edoff, T. Jarmar, N. S. Nilsson, E. Wallin, D. Högström, O. Stolt, O. Lundberg, W. Shafarman, and L. Stolt, IEEE J. Photovolt. **7**, 1789 (2017). DOI: 10.1109/JPHOTOV.2017.2756058.
29. S. A. Moiz, Photonics **9**, 23 (2022). DOI: 10.3390/photonics9010023.
30. D. P. Pham, S. Lee, Y. Kim, and J. Yi, J. Phys. Chem. Sol. **154**, 110059 (2021). DOI: 10.1016/j.jpcs.2021.110059.
31. R. L. Z. Hoye, M. R. Chua, K. P. Musselman, G. Li, M.-L. Lai, Z.-K. Tan, N. C. Greenham, J. L. Macmanus-Driscoll, R. H. Friend, and D. Credgington, Adv. Mater. **27**, 1414 (2015). DOI: 10.1002/adma.201405044.
32. H. Li, Z.-G. Zhang, Y. Li, and J. Wang, Appl. Phys. Lett. **101**, 163302 (2012). DOI: 10.1063/1.4761246.
33. W. Bagienski, G. S. Kinsey, M. Liu, A. Nayak, and V. Garboushian, AIP Conf. Proce. **1477**, 148 (2012). DOI: 10.1063/1.4753855.
34. Mamta, K. K. Maurya, and V. N. Singh, Sustainability **13**, 12320 (2021). DOI: 10.3390/su132112320.

تحسين عدة معلمات من خلايا البيروفسكايت الشمسية نحو كفاءة 30% باستخدام SCAPS-1D

براق يحيى كاظم[1] واحسان محسن عباس[2]
[1]كلية العلوم، جامعة الكرخ للعلوم، بغداد، العراق
[2]كلية التقنيات الصحية والطبية، جامعة الشعب، بغداد، العراق

الخلاصة

تم فحص خلية شمسية محاكاة من البيروفسكايت تعتمد على بنية P3HT/MAPbI3/C60 لتحقيق كفاءة تحويل طاقة بنسبة 30% باستخدام برنامج SCAPS-1D. تم تقييم العديد من جوانب الطبقة النشطة من البيروفسكايت، بما في ذلك السُمك، ونطاق التوصيل (C_B) ونطاق التكافؤ (V_B) والكثافة الفعالة للحالة، وفجوة النطاق (E_g)، وتقارب الإلكترون (E_A). تظهر هذه العوامل تأثيرًا كبيرًا على أداء الجهاز. أظهر أفضل أداء للجهاز بناءً على أفضل معلمة تم فحصها PCE بنسبة 32.1% مرتبطة بعامل التعبئة (FF) بنسبة 84.8%، وجهد الدائرة المفتوحة (1.23) VOC فولت وكثافة تيار الدائرة القصيرة (30.77) JSC مللي أمبير. سم$^{-2}$. هذه النتيجة واعدة فيما يتعلق بالقدرة على تحقيق PCE عالية للخلايا الشمسية القائمة على البيروفسكايت من خلال تحسين العديد من العوامل، بما في ذلك سُمك الطبقة النشطة، وفجوة نطاق الطاقة، وتقارب الإلكترون، والكثافة الفعالة للحالة لـ C_B وV_B. ومع ذلك، بالنسبة للخلايا الشمسية المنتجة تجريبياً، فإن ظروف التحضير وعوامل أخرى قد تؤدي إلى هذه النتيجة. إن كثافة الحالة الفعالة المنخفضة ($1x10^{16}m^{-3}$) مطلوبة لكل من CB وVB لتحقيق أداء عالٍ للخلايا الشمسية.

الكلمات المفتاحية: الخلايا الشمسية، MAPbI، مادة البيروفسكايت، SCAPS-1D، P3HT.